where x approaches zero along the positive imaginary axis. Using equations (C.31) and (C.13) to evaluate the limit in equation (2.203), we then find (Hunter 1963)

$$\Sigma_{lm} = -\frac{2V_{lm}}{\pi^2 G\Delta g_{lm}} \frac{\mathrm{Y}_l^m(v,\phi)}{|\cos v|}, \tag{2.204a}$$

where

$$g_{lm} \equiv \frac{(l+m)!(l-m)!}{2^{2l-1}\left[\left(\frac{l+m}{2}\right)!\left(\frac{l-m}{2}\right)!\right]^2}. \tag{2.204b}$$

A general disk potential, which is a sum over l and m of potentials of the form (2.202), is generated by the surface density $\Sigma(v,\phi)$ that is the sum of surface densities $\Sigma_{lm}(v,\phi)$. According to equation (2.204a), $-2V_{lm}/(\pi^2 G\Delta g_{lm})$ is the coefficient of $\mathrm{Y}_l^m(v,\phi)$ when $|\cos v|\Sigma(v,\phi)$ is expanded in spherical harmonics. Thus with the orthogonality relation (C.44) we have

$$\frac{2V_{lm}}{\pi^2 G\Delta g_{lm}} = -\int_0^{2\pi} \mathrm{d}\phi \int_0^{\pi} \mathrm{d}v\, \sin v\, |\cos v|\Sigma(v,\phi)\mathrm{Y}_l^{m*}(v,\phi). \tag{2.205}$$

The integrand in equation (2.205) is symmetrical about $v = \pi/2$ when $l-m$ is even, so we may restrict the v integration to the range $(0,\pi/2)$ and double the result. Hence

$$V_{lm} = -\frac{\pi^2 G g_{lm}}{\Delta} \int_0^{2\pi} \mathrm{d}\phi \int_0^{\Delta} \mathrm{d}R\, R\Sigma(R,\phi)\mathrm{Y}_l^{m*}\Big(\sin^{-1}(R/\Delta),\phi\Big). \tag{2.206}$$

All the techniques in this section are special cases of a general method for finding disk potential-density pairs that is described by Qian (1992).

2.7 The potential of our Galaxy

In this section we investigate the gravitational field of our own galaxy, the Milky Way. The Galaxy is made of several components, the disk, the bulge, the stellar halo, and the dark halo. The mix of stars, gas and dark matter that makes up a galaxy such as our own varies from component to component and is even likely to depend on location within each component.

Ideally, we should rely solely on dynamical tracers, such as the velocity fields of gas and stars and observations of gravitational lensing, to map out the distribution of mass in the Galaxy. Sadly, at the present time such a project is unfeasible.

Since we are not yet in a position to model the Galactic density and gravitational field in a purely dynamical way, we flesh out the available dynamical constraints with photometric information. In particular, we simply

assume that each component has a mass-to-light ratio Υ that is independent of position. For the reason given above, this procedure is arbitrary and unsatisfactory, but it yields concrete Galactic potentials, which make testable predictions regarding the kinematics of stars and gas. Proceeding in this spirit, we now investigate models of our Galaxy, following Dehnen & Binney (1998a) and BM §10.6.

The brightness distribution of each component is assumed to be similar to those of external galaxies (BM §§4.3 and 4.4), while the size and total luminosity of each component is determined from photometry and star counts, or by fitting to the available dynamical constraints. We do not model the stellar halo here since its contribution to the potential is negligible.

The models are constrained by fitting to the following data (cf. Table 1.2):

(i) The circular-speed curve $v_{\rm c}(R)$ for an assumed value of the solar circular speed, $v_0 \equiv v_{\rm c}(R_0)$. Since this curve is determined from the line-of-sight velocities of tracers such as HI clouds and Cepheid stars, the circular-speed curve depends on v_0, which must be determined by other methods.
(ii) The values of the Oort constants (Table 1.2, eq. 3.83, and BM §10.3.3).
(iii) The total surface density within 1.1 kpc of the Galactic plane near the Sun, $\Sigma_{1.1}(R_0)$, and the contribution of the disk to this density (Table 1.1).
(iv) The velocity dispersion of bulge stars in Baade's window, a line of sight that passes $\sim 500\,$pc from the Galactic center in which absorption by intervening dust is unusually low. We take this dispersion to be $117 \pm 15\,{\rm km\,s^{-1}}$.
(v) The total mass within 100 kpc of the Galactic center (eq. 1.12).
(vi) The solar radius $R_0 = 8\,$kpc.

The functional forms assumed for each of the Galaxy's components are as follows.

(a) The bulge The density of this component is assumed to be

$$\rho_{\rm b}(R,z) = \rho_{\rm b0}\Big(\frac{m}{a_{\rm b}}\Big)^{-\alpha_{\rm b}} {\rm e}^{-m^2/r_{\rm b}^2}, \tag{2.207a}$$

where

$$m = \sqrt{R^2 + z^2/q_{\rm b}^2}. \tag{2.207b}$$

For $q_{\rm b} < 1$ this is an oblate, spheroidal power-law model that is truncated at an outer radius $r_{\rm b}$. Its potential is conveniently calculated from equations (2.125) with

$$e = \sqrt{1-q_{\rm b}^2} \quad ; \quad \psi(m) = \rho_{\rm b0} \int_0^m {\rm d}m^2 \left(\frac{m}{a_{\rm b}}\right)^{-\alpha_{\rm b}} {\rm e}^{-m^2/r_{\rm b}^2}. \tag{2.208}$$

Near-infrared photometry (BM §10.2.1) suggests values for three of the parameters, $\alpha_{\rm b} = 1.8$, $q_{\rm b} = 0.6$, $r_{\rm b} = 1.9\,$kpc, and without loss of generality,

we can set $a_{\rm b} = 1\,{\rm kpc}$. The parameter $\rho_{\rm b0}$, and hence the mass of the bulge, are determined by fitting the dynamical constraints.

(b) The dark halo By extending the spherical two-power-law models of §2.2.2f to oblate models, the density of this component is taken to have the form

$$\rho_{\rm h}(R,z) = \rho_{\rm h0}\Big(\frac{m}{a_{\rm h}}\Big)^{-\alpha_{\rm h}}\Big(1+\frac{m}{a_{\rm h}}\Big)^{\alpha_{\rm h}-\beta_{\rm h}}, \tag{2.209}$$

where m is again given by equation (2.207b) with $q_{\rm b}$ replaced by $q_{\rm h}$. The potential of this component, in which the density varies as $r^{-\alpha_{\rm h}}$ for $r \ll a_{\rm h}$ and $r^{-\beta_{\rm h}}$ at large r, can also be obtained from equation (2.125). Clearly, photometry provides no guidance as to the values of any of the parameters in equation (2.209); all five parameters $\rho_{\rm h0}$, $a_{\rm h}$, $\alpha_{\rm h}$, $\beta_{\rm h}$, and $q_{\rm h}$ can only be determined by fitting the dynamical constraints. The data we use have little sensitivity to $q_{\rm h}$, and we arbitrarily set it to 0.8.

(c) The stellar disk The density of the stellar disk is assumed to fall off exponentially with radius R, as in equation (1.7), and to depend on distance from the midplane z through the sum of two exponentials, representing the thin and thick disks described on page 13—this dependence on z is motivated by observations such as those of Gilmore & Reid (1983), shown in BM Figure 10.25. Mathematically,

$$\rho_{\rm d}(R,z) = \Sigma_{\rm d}{\rm e}^{-R/R_{\rm d}}\left(\frac{\alpha_0}{2z_0}{\rm e}^{-|z|/z_0} + \frac{\alpha_1}{2z_1}{\rm e}^{-|z|/z_1}\right), \tag{2.210}$$

where $\alpha_0 + \alpha_1 = 1$, $\Sigma_{\rm d}$ is the central surface density, $R_{\rm d}$ is the disk scale length, and $z_0 = 0.3\,{\rm kpc}$ and $z_1 = 1\,{\rm kpc}$ are scale heights for the thin and thick components. The potential generated by this density distribution is given by equation (2.170) with $\zeta(z)$ replaced by the expression in large brackets in equation (2.210).

(d) The interstellar medium The disk formed by a galaxy's interstellar medium (ISM) is thinner and more extended radially than the galaxy's stellar disk (see, for example, BM Figures 8.25 and 9.19). In the case of the Milky Way there is a hole of radius $\sim 4\,{\rm kpc}$ at the center of the disk of the ISM (BM Figure 9.19). These observations are crudely represented by taking the density of the ISM to be

$$\rho_{\rm g}(R,z) = \frac{\Sigma_{\rm g}}{2z_{\rm g}}\exp\Big(-\frac{R}{R_{\rm g}} - \frac{R_{\rm m}}{R} - \frac{|z|}{z_{\rm g}}\Big), \tag{2.211}$$

with $R_{\rm m} = 4\,{\rm kpc}$ and $z_{\rm g} = 80\,{\rm pc}$. The parameters $\Sigma_{\rm g}$ and $R_{\rm g}$ are related to the parameters $\Sigma_{\rm d}$ and $R_{\rm d}$ of equation (2.210) by the assumption that $R_{\rm g} = 2R_{\rm d}$ and that the ISM contributes 25% of the total disk surface density

Table 2.3 Parameters of Galaxy models

Parameter	Model I	Model II
$R_{\rm d}/{\rm kpc}$	2	3.2
$(\Sigma_{\rm d}+\Sigma_{\rm g})/\mathcal{M}_\odot\,{\rm pc}^{-2}$	1905	536
$\rho_{\rm b0}/\mathcal{M}_\odot\,{\rm pc}^{-3}$	0.427	0.3
$\rho_{\rm h0}/\mathcal{M}_\odot\,{\rm pc}^{-3}$	0.711	0.266
$\alpha_{\rm h}$	-2	1.63
$\beta_{\rm h}$	2.96	2.17
$a_{\rm h}/{\rm kpc}$	3.83	1.90
$M_{\rm d}/10^{10}\,\mathcal{M}_\odot$	5.13	4.16
$M_{\rm b}/10^{10}\,\mathcal{M}_\odot$	0.518	0.364
$M_{\rm h,<10\,kpc}/10^{10}\,\mathcal{M}_\odot$	2.81	5.23
$M_{\rm h,<100\,kpc}/10^{10}\,\mathcal{M}_\odot$	60.0	55.9
$v_{\rm e}(R_0)/{\rm km\,s}^{-1}$	520	494
$f_{\rm b}$	0.05	0.04
$f_{\rm d}$	0.60	0.33
$f_{\rm h}$	0.35	0.63

NOTES: In both models $0.75\Sigma(R_0)$ is contributed by stars, of which $0.05\Sigma(R_0)$ is in the thick disk. Interstellar gas accounts for the remaining $0.25\Sigma(R_0)$. The thin and thick disks have the same scale length $R_{\rm d}$, while the gas disk has scale length $2R_{\rm d}$ and a central hole of radius $R_{\rm m}=4\,{\rm kpc}$. The thicknesses of the disks are $z_0=300\,{\rm pc}$, $z_1=1\,{\rm kpc}$, $z_{\rm g}=80\,{\rm pc}$. In both models the bulge parameters are $a_{\rm b}=1\,{\rm kpc}$, $\alpha_{\rm b}=1.8$, $r_{\rm b}=1.9\,{\rm kpc}$, $q_{\rm b}=0.6$, while the halo axis ratio $q_{\rm h}=0.8$. The quantity $v_{\rm e}(R_0)$ is the escape speed from the solar neighborhood; $f_{\rm b}$, $f_{\rm d}$ and $f_{\rm h}$ are the fractions of the radial force supplied by bulge, disk and halo at $R_0=8\,{\rm kpc}$. These are slightly modified forms of Models 1 and 4 of Dehnen & Binney (1998a).

at the solar radius, R_0. The potential implied by equation (2.211) is best found from equation (2.154).

Dehnen & Binney (1998a) found that fits to the constraints described above could be obtained for a wide range of models made up of the components (a) to (d). The most important single parameter for determining the properties of a model is the scale length of the stellar disk, $R_{\rm d}$. In §1.1.2 we estimated that $R_{\rm d}$ lies between 2 and 3 kpc. When $R_{\rm d}$ is at the lower end of this range, the disk dominates the gravitational field out to beyond the solar radius, whereas when $R_{\rm d}=3\,{\rm kpc}$, the halo dominates at all radii. It is useful to examine the properties of two extreme models, namely the most and the least halo-dominated models; we designate them Models I and II and list their parameters in Table 2.3.

Model I has a small scale length, $R_{\rm d}=2\,{\rm kpc}$, and gives rise to the isopotential surfaces and circular-speed curves shown in Figures 2.19 and 2.20. At small radii the halo density is $\rho_{\rm h}\propto r^{-\alpha_{\rm h}}=r^2$, which is the smallest value of $\alpha_{\rm h}$ allowed by the fitting program—with this disk scale length, the best fit has the smallest possible halo contribution near the center. Figure 2.20 illus-

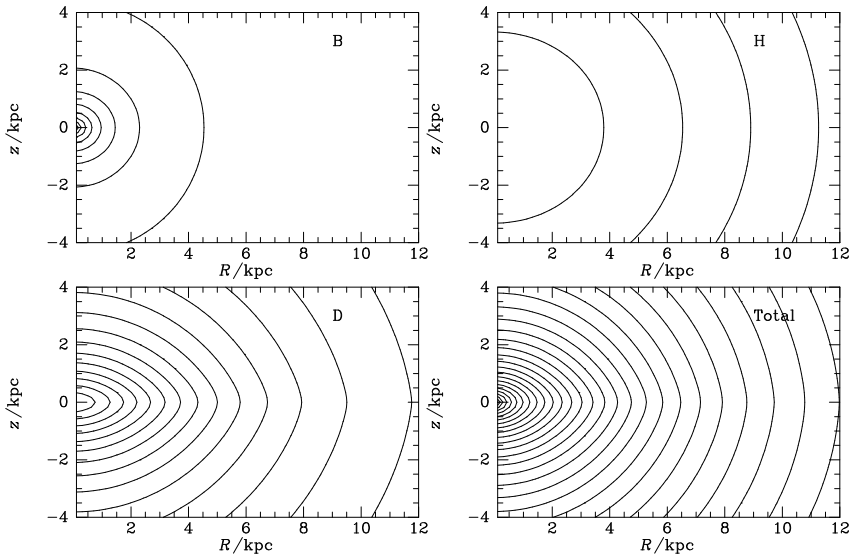

Figure 2.19 The lower right panel shows equipotential contours of a model of the Galaxy with $R_{\rm d} = 2\,{\rm kpc}$ (Model I). Contour levels are $(-0.5, -1, -1.5\ldots) \times (100\,{\rm km\,s^{-1}})^2$. The top left panel shows the potential of the bulge, while the potentials of halo and disk are shown at top right and lower left, respectively. From top left to lower right the potentials at $(R, z) = (8\,{\rm kpc}, 0)$ are -0.28, -10.2, -2.98, $-13.46 \times (100\,{\rm km\,s^{-1}})^2$.

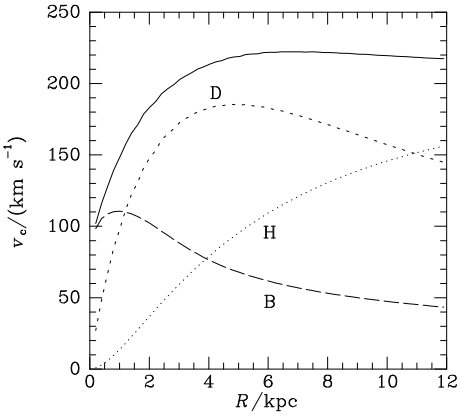

Figure 2.20 The full curve shows the circular-speed curve of Model I, whose potential is contoured in Figure 2.19. The contributions from the bulge, halo and disk are shown by the long-dashed, dotted and short-dashed curves, respectively. Notice that the total circular speed is given by the sum in quadrature of the circular speeds of the components.

trates the dynamical importance of the disk and bulge interior to the solar radius, showing that at such radii the halo makes only a small contribution to the overall circular speed—since $v_{\rm c}^2 \propto g$, the contribution to the gravitational force is even smaller. This dominance is reflected in the contour plots of Figure 2.19 by the much closer packing of the equipotential contours of the bulge (top left panel) and disk (lower left panel) than those of the halo (top right panel). The equipotential surfaces of the disk are naturally more

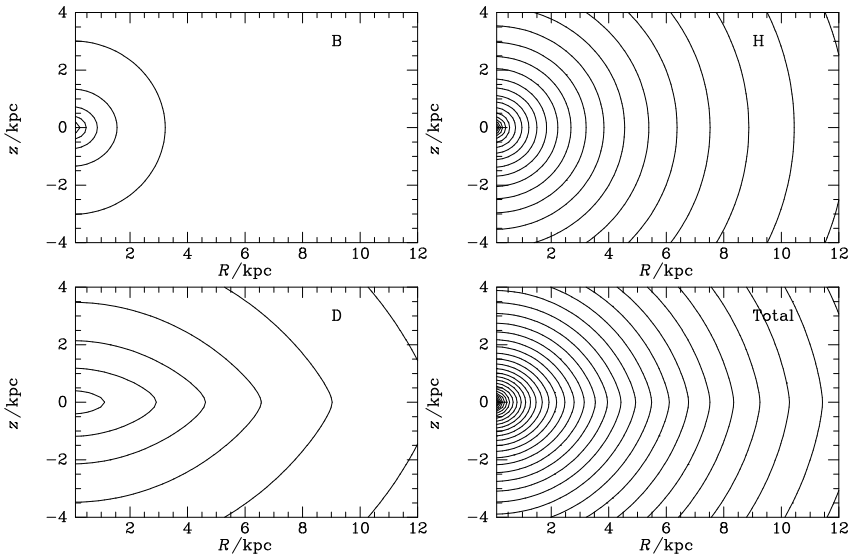

Figure 2.21 Equipotential contours of the halo-dominated Galaxy model, Model II, which has $R_{\rm d} = 3.2\,{\rm kpc}$. The top left panel shows the potential of the bulge, while the potentials of halo and disk are shown at top right and lower left, respectively. The lower right panel shows the overall potential with contour levels $(-0.5, -1, -1.5\ldots) \times (100\,{\rm km\,s^{-1}})^2$. From top left to lower right the potentials at $(R, z) = (8\,{\rm kpc}, 0)$ are -0.20, -9.83, -2.19, $-12.21 \times (100\,{\rm km\,s^{-1}})^2$.

highly flattened than those of either the bulge or the halo, so the equipotential surfaces of the total potential are most flattened at radii $r \sim 5\,{\rm kpc}$, where the disk's potential dominates.

Although in Model I the disk dominates the gravitational field (potential gradient) at R_0, the halo makes by far the largest contribution to the total potential at all radii. For example, at the Sun's location the halo contributes $-10.2 \times (100\,{\rm km\,s^{-1}})^2$ to the overall potential, while the disk and bulge together contribute only $-3.26 \times (100\,{\rm km\,s^{-1}})^2$. The large contribution from the halo reflects the its enormous mass, most of it beyond R_0. Just how much mass the halo contains is ill-determined because the Galaxy's circular speed $v_{\rm c}(R)$ is uncertain beyond $\approx 2R_0$.

Figures 2.21 and 2.22 analyze the potential of Model II, a model that has a larger disk scale length, $R_{\rm d} = 3.2\,{\rm kpc}$. As Figure 2.22 shows, in this model the halo dominates the circular speed at all radii. It does so because it is much more centrally concentrated than the halo of Model I: at small r its density rises towards the center as $r^{-1.63}$ rather than falling as in Model I. At the solar position the escape speed in this model is $v_{\rm e}(R_0) = 494\,{\rm km\,s^{-1}}$, which is observationally indistinguishable from $v_{\rm e}(R_0) = 520\,{\rm km\,s^{-1}}$ in Model I; both are consistent with the observational estimate $v_{\rm e}(R_0) = (550 \pm 50)\,{\rm km\,s^{-1}}$ in Table 1.2.

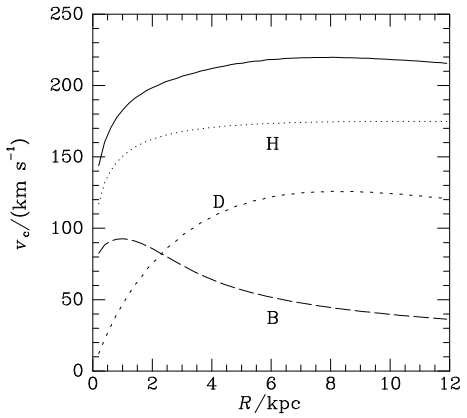

Figure 2.22 The full curve shows the circular-speed curve of Model II. The contributions from the bulge, halo and disk are shown by the long-dashed, dotted and short-dashed curves, respectively.

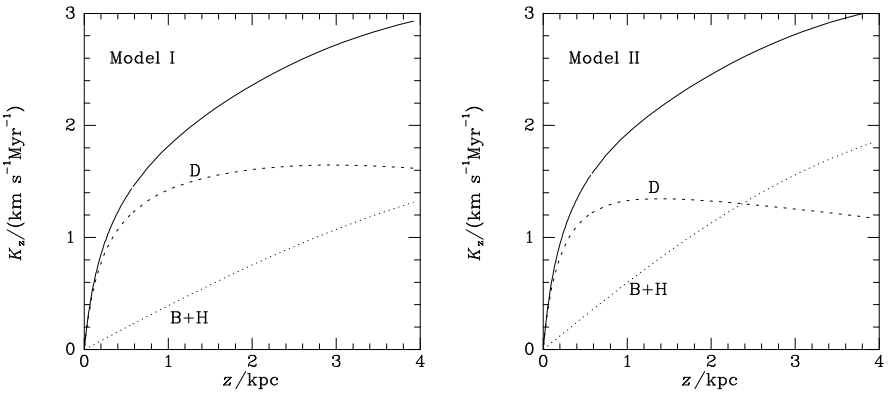

Figure 2.23 In each panel the full curve shows as a function of z in a Galactic model the force towards the galactic plane, $K_z = \partial\Phi/\partial z$ at $R_0 = 8\,\mathrm{kpc}$. The contributions from the bulge plus halo and disk are shown by the dotted and dashed curves, respectively. The left panel is for disk-dominated model, Model I (Figures 2.19 and 2.20), while the right panel is for Model II (Figures 2.21 and 2.22).

One of the striking conclusions from these models is that the relative contributions of the disk and the halo to the interior mass and the circular speed at R_0 are very uncertain. As R_d varies from 3.2 kpc to 2 kpc, the mass of the dark halo inside 10 kpc decreases by nearly a factor 2 and the fraction of the gravitational force at R_0 contributed by the halo falls[9] from 0.63 to 0.35. Similar uncertainties are encountered in models of external disk galaxies (van Albada et al. 1985; Sellwood 1999). This degeneracy between the disk and halo parameters has to be resolved by bringing other observational constraints or dynamical arguments to bear, such as those obtained from measurements of the dynamics of galactic bars (§6.5.2e), and

[9] Models in which most of the force at $\sim 2R_\mathrm{d}$ comes from the disk are called "maximum-disk models"—see §6.3.3.

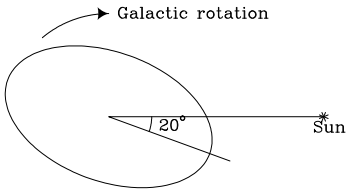

Figure 2.24 Schematic diagram of the Galactic bar.

the optical depth to gravitational microlensing towards the Galactic center (Bissantz & Gerhard 2002; Famaey & Binney 2005).

Even though the halo of Model II dominates the circular speed at R_0, Figure 2.23 shows that the vertical force towards the disk, $K_z = \partial\Phi/\partial z$, is dominated by the disk within $\sim 2\,\mathrm{kpc}$ of the plane. Even a relatively low-mass disk can dominate K_z in this way because a disk's contribution to K_z rises extremely quickly near the plane, where the density of disk material is high. Above one scale height, $\sim 200\,\mathrm{pc}$, the disk's contribution to K_z flattens off to the nearly constant value $2\pi G\Sigma(R)$ (cf. Problem 2.3). By contrast, in both panels of Figure 2.23 the halo's contribution to K_z (dotted curves) rises nearly linearly with z out to several kiloparsecs above the Sun. Notice how similar the full curves in Figure 2.23 are: despite the very different contributions to v_c from disk and halo in the two models, the shape of the observationally measurable quantity K_z (§4.9.3) is almost the same in the two cases.

(e) The bulge as a bar There is both kinematic and photometric evidence that the Milky Way's bulge is in fact a bar, that is, a highly elongated, rapidly rotating stellar system (§6.5 and BM §§9.4 and 10.1). From the vantage point of the Sun, it is hard to determine the precise shape of the bar, but, as sketched in Figure 2.24, the bar is believed to extend to a Galactocentric radius $\sim 3\,\mathrm{kpc}$, with its longest axis inclined by about 20° to the line from the Sun to the Galactic center (Bissantz & Gerhard 2002). The lengths of the bar's semi-axes are roughly in the ratios $1:0.3:0.3$.

Both photometric studies of the bar itself and comparisons with bars in other galaxies suggest that the isodensity surfaces deviate significantly from ellipsoids (López–Corredoira et al. 2005). Nonetheless, when considering the impact that the bar has on the Galaxy's gravitational potential, it is useful to start by approximating the isodensity surfaces by ellipsoids for in this case we can obtain the potential from equation (2.140)—if a more exact result were required, one could expand the difference $\rho(\mathbf{x}) - \rho_\mathrm{e}(\mathbf{x})$ between the actual density distribution ρ and the elliptical model ρ_e in spherical harmonics, and obtain the small correction to the potential from equation (2.95). In this spirit, we estimate the effect of the bar on the Galaxy's potential by fashioning a bar out of the axisymmetric bulge of Model I as follows.

In equations (2.207) we increase the scale radius r_b from 1.9 kpc to 3 kpc, and redefine m by $m^2 = x^2 + (y^2 + z^2)/q^2$, where x runs along the bar's long axis. We adopt $q = 0.35$ and increase ρ_0 so that the bar has roughly the same mass as the original bulge. In Figure 2.25 the full curves show the

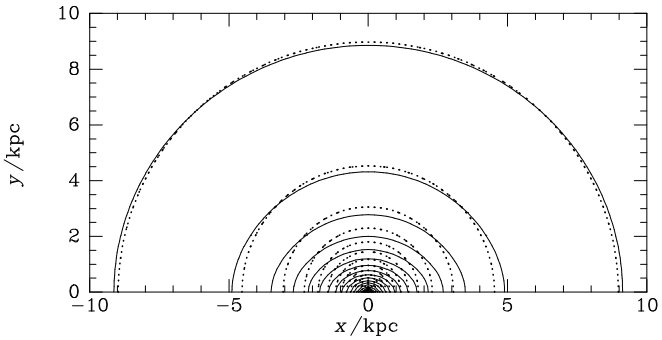

Figure 2.25 Full curves show the intersection with the Galactic plane of the isopotential surfaces of a model of the galactic bar. For comparison the dotted curves show the same curves for the axisymmetric bulge of Model I.

intersection with the Galactic plane of the bar's isopotential surfaces, while the dotted curves show the corresponding curves for the bulge of Model I. As expected, the bar's isopotential surfaces are elongated. The effect is very small near the solar circle but appreciable at $R \lesssim 5\,\mathrm{kpc}$. On account of this elongation, the potential now generates tangential forces: Along a radius that makes an angle of 45° with the bar's long axis, the ratio F_ϕ/F_r of the tangential and radial forces from the bar falls from 0.4 at the center to 0.27 at 2 kpc and 0.125 at 4 kpc. From Figure 2.20 we see that the bulge dominates F_r at $R \lesssim 1\,\mathrm{kpc}$, so in this crude model tangential forces are very important at small radii. Conversely, at $R \simeq 4\,\mathrm{kpc}$ the bulge contributes only 11% of F_r, so at that radius F_ϕ is only $\sim 1\%$ of F_r. Nonetheless, the tangential forces that the bar induces can be dynamically significant for resonant orbits as far out as the solar circle because along such orbits the effect of F_ϕ can accumulate over several periods (§3.7.2 and Dehnen 2000a).

We conclude that accurate models of the triaxial bar are needed to understand the dynamics of the Milky Way at $R \lesssim 2$–$3\,\mathrm{kpc}$, and possibly beyond.

2.8 Potentials from functional expansions

A common theme of many of the methods we have described is the expansion of the gravitational potential and density in a set of functions that are potential-density pairs. We shall encounter such methods again in §2.9.4 as efficient tools for N-body simulation, and in §5.3.2, where we study linear response theory for stellar systems. In this section we re-examine these techniques from a general standpoint.

The basic idea of §2.3 was to approximate a real galactic density distribution by a density for which the potential is known analytically. Only a